Author Manuscript

Author Manuscript

Author Manuscript

Author Manuscript

HHS Public Access

Author manuscript

Cancer Res. Author manuscript; available in PMC 2016 October 15.

Published in final edited form as:

Cancer Res. 2015 October 15; 75(20): 4302–4311. doi:10.1158/0008-5472.CAN-14-3331.

STAT3 blockade inhibits a radiation-induced proneural-to-mesenchymal transition in glioma

Jasmine Lau[1,2,3], **Shirin Ilkhanizadeh**[1,2,3], **Susan Wang**[2,3,4], **Yekaterina A. Miroshnikova**[5], **Nicolas A. Salvatierra**[1,2,3], **Robyn A. Wong**[1,2,3], **Christin Schmidt**[1,2,3], **Valerie M. Weaver**[3,5,6], **William A. Weiss**[1,2,3,*], and **Anders I. Persson**[2,3,4,*]

[1] Departments of Pediatrics, University of California, San Francisco, San Francisco, CA 94158

[2] Department of Neurology, Neurological Surgery and Brain Tumor Research Center, University of California, San Francisco, San Francisco, CA 94158

[3] Helen Diller Family Comprehensive Cancer Center, University of California, San Francisco, San Francisco, CA 94158

[4] Sandler Neurosciences Center, University of California, San Francisco, San Francisco, CA 94158

[5] Department of Surgery and Center for Bioengineering and Tissue Regeneration, University of California, San Francisco, San Francisco, CA 94143

[6] Departments of Anatomy and Bioengineering and Therapeutic Sciences, and Eli and Edythe Broad Center of Regeneration Medicine and Stem Cell Research, University of California, San Francisco, San Francisco, CA 94143

Abstract

Malignant progression is often associated with a mesenchymal phenotype and poor prognosis. To test whether radiotherapy promotes a mesenchymal transition, we irradiated proneural tumors arising in a genetically engineered mouse model for high-grade glioma. Cranial ionizing radiation induced a robust and durable proneural-to-mesenchymal transition in tumors. Radiation of primary proneural high-grade glioma cells derived from mouse and human tumors also induced a sustained cell-intrinsic mesenchymal transition, associated with increased invasiveness and resistance to the alkylating agent temozolomide. The transcription factor STAT3 was activated in response to irradiation, and blockade of STAT3 abrogated the mesenchymal transition and combination treatment of JAK2 inhibitors with radiation extended survival in mice. Our data suggest that clinical JAK2 inhibitors should be tested in conjunction with radiation in patients with proneural high-grade glioma, to block emergence of therapy-resistant mesenchymal tumors at relapse.

[*]**Corresponding Authors**: William A. Weiss, Helen Diller Family Comprehensive Cancer Center, University of California, San Francisco, 1450 3rd Street, MC 0520, Room 277, San Francisco, CA 94158-9001, Tel: (415) 502-1694, Fax: (415) 476-0133, waweiss@gmail.com, Anders I. Persson, Sandler Neurosciences Center, Box 3208, University of California, San Francisco, 675 Nelson Rising Lane, Room NS-270B, San Francisco, CA 94158, Tel: (415) 502-7178, anders.persson@ucsf.edu.

The authors disclose no potential conflicts of interest.

Author Manuscript Author Manuscript Author Manuscript Author Manuscript

Keywords

STAT3; radiation; glioma; mesenchymal; proneural

Introduction

Malignant high-grade gliomas (HGGs) are highly lethal brain tumors that include anaplastic oligodendroglioma, anaplastic astrocytoma, and glioblastoma (GBM). The introduction of radiotherapy improved median survival of HGG patients from six months to one year (1,2). In addition to radiation, multimodal therapy includes surgical resection and systemic treatment with alkylating agents (2-4). Despite treatment however, patients with HGGs invariably relapse and recurrent tumors are typically refractory to further therapies.

Transcriptional profiling has categorized HGGs into distinct groups, represented as a continuum between proneural and mesenchymal subclasses (5-9). The mesenchymal signature correlates with poor prognosis when compared with proneural tumors (10), and proneural tumors tend to shift to a mesenchymal signature at recurrence (5,11-13). The proneural-to-mesenchymal transition (PMT) is enriched for genes associated with an epithelial-to-mesenchymal transition (EMT) (14,15), and likely represents an analogous process. Genes important in the mesenchymal phenotype in HGGs include transcription factors CEBPβ, STAT3 (16), TAZ (17), NFκB (10), and ID proteins (18). Signals from the microenvironment also activates the mesenchymal phenotype, which is enriched in genes associated with inflammation, necrosis and angiogenesis (6,10,19).

Radiation may contribute to a PMT in glioma. Transcriptional profiling of PDGFB-driven murine glioma cells isolated 6 hr post-irradiation revealed a mesenchymal shift in gene expression (20). While durability of radiation-induced PMT in glioma has not been addressed *in vivo*, radiation of cultured human proneural GBM cells induced a PMT that was sustained for at least five days (21). If radiation therapy in patients induces a sustained mesenchymal switch in the remaining radioresistant cells, blocking this transition may prevent relapse, or block therapy resistance in relapsed tumors.

Here, we radiated proneural HGG in a genetically engineered glioma mouse model, demonstrating a durable PMT. Radiation-induced PMT occurred in a cell-intrinsic manner, resulting in increased cell motility and invasion, and was associated with resistance to the alkylating agent temozolomide. Importantly, STAT3 signaling was induced in radiated cells, and pharmacological inhibition of STAT3 using clinical agents effectively prevented PMT. Our results suggest that radiotherapy as part of standard of care for patients with proneural HGG may contribute to a PMT in recurrent tumors, and that blockade of JAK2-STAT3 signaling may prevent PMT and recurrence, increasing the survival of HGG patients.

Materials and Methods

Mice

All mouse experiments were approved by and performed according to the guidelines of the Institutional Animal Care and Use Committee of the University of California, San

Author Manuscript Author Manuscript Author Manuscript Author Manuscript

Francisco. Mice were genotyped by Transnetyx, Inc. ERB/p53$^{-/-}$ proneural HGG mice were genotyped for S100β-verbB transgene and wild-type or null mutation of p53 using the protocol as previous published (22,24). GFAPHA-V12-Ras-IRESLacZ mice were genotyped as previously published (23).

Tissue preparation

Mice were perfused transcardially using PBS followed by 4% paraformaldehyde (PFA). Brains were harvested and incubated overnight in 4% PFA at 4°C, and transferred to 30% sucrose at 4°C. Brains were sectioned using a cryostat (Leica) as 30 μm free-floating sections. Sections were stored in cryoprotectant solution (25% glycerol, 25% ethylene glycol, 50% 0.1 M phosphate buffer) at −20 °C until immunostaining procedure.

Immunofluorescence

Free-floating sections were retrieved from cryoprotectant solution and washed 3x10 min in Tris-buffered saline (TBS, pH 7.4). The sections were then incubated in blocking solution (5% donkey serum, 1% BSA, 0.3% TritonX-100) for 1 h at room temperature. Primary antibodies were diluted in blocking solution and incubated on sections overnight at 4°C. Antibodies used: SOX10 (1:200, Santa Cruz Biotechnology), PDGFRα (1:200, Cell Signaling), CD44 (1:400, BD Pharmingen). Sections were washed in TBS, and incubated with the appropriate Alexa488 (1:400), 555 (1:400), 647 (1:200) secondary antibodies (Life Technologies) in blocking solution for 2 h at room temperature. The sections were washed in TBS 3×10 min (DAPI was included in the second wash), following by mounting with ProLong Gold antifade reagent (Life Technologies).

Imaging and Quantification

Mosaic images were acquired and tiled using the Zeiss M1 AxioImager and the Zen software. For quantification, tumor regions (DAPI bright) were identified, and region of interest was determined, avoiding areas at the edge of tumor/section and necrotic regions. The mean fluorescence intensity was determined using the image analysis tool.

Western blotting

For tissue specimens, samples were frozen in dry ice and stored at −80°C until processed. Samples were homogenized and sonicated in cell lysis buffer (Cell Signaling). For cells, samples were washed in ice-cold PBS before lysis with cell lysis buffer (Cell Signaling). All samples were clarification by centrifugation at 16,000 rpm for 10 min at 4°C and quantified using the Pierce BCA protein assay kit (Thermo Scientific). Equal amounts of total protein lysates were loaded and resolved on a 4-12% Bis-Tris Gel with MOPS Running buffer and transferred to PVDF membranes. The membranes were blotted with antibodies against PDGFRα, pSTAT3 (Tyr705), STAT3 (all from Cell Signaling), CD44 (Thermo Scientific), SOX10 (Santa Cruz Technologies) and GAPDH (Millipore). Bound antibodies were detected with horseradish peroxidase-linked antibody against mouse (Calbiochem), rabbit (Calbiochem) or goat (Santa Cruz Technology) immunoglobulin G, followed by ECL (Amersham).

Author Manuscript Author Manuscript Author Manuscript Author Manuscript

Quantitative PCR analysis

Dissected tissue samples or cells were homogenized using the QIAshredder spin column (Qiagen). Total RNA was extracted from specimens using RNeasy mini kit (Qiagen) and contaminating RNA was digested using RNase free DNase kit (Qiagen). cDNA was synthesized using 500 ng total RNA using High Capacity cDNA Reverse Transcription Kit (Applied Biosystems) or SuperScript VILO (Life Technologies). Real time PCR was performed with the intron-spanning primers (5 μM) listed below and KAPA SYBR fast ABI prism qPCR master mix (KAPA biosystems) on a 7900 HT Fast Real-Time PCR system (Applied Biosystems).

Gene	Forward primer	Reverse primer
mSox10	GTGCCAGCAAGAGCAAGCCG	CTGCCTTCCCGTTCTTCCGCC
mPdgfra	ACAGCCGAAGGCACCCCTCT	CTCACGGGCCACAACGCTGA
mCD44	TCGTTGCCCTTCTCCCCACGA	CCTGCGTAGCGGCAGGTTACA
mChi3l1	AGGCCATCACAGCCCCCTCTT	ACCTTCTCGTTGGAGAGTCGATGT
mTgfb1	AACCCCCATTGCTGTCCCGTG	GCGCTGAATCGAAAGCCCTGT
mFn1	GGCTACATCATCCGCCATCA	TAATAGCGCACAGAGACGGC
mVim	AAGCTGCTGGAAGGCGAGGAGA	CTTCTTGCTGGTACTGCACTGTTGC
mSlug	CACATTCGAACCCACACATTGCCT	TGTGCCCTCAGGTTTGATCTGTCT
mPDPN	TGGGGAGCGTTTGGTTCTGGG	CCACGCTCTCTCTGCGTTGGT
mSnail	TTGTGTCTGCACGACCTGTGGAAA	TCTTCACATCCGAGTGGGTTTGGA
mTwist	GCTACGCCTTCTCCGTCTGG	CCCTGATTCTTGTGAATTTGGTCTC
mHprt	CTTCCTCCTCAGACCGCTTTTT	ATGTAATCCAGCAGGTCAGCAA
mGapdh	GTGCAGTGCCAGCCTCGTCC	CAGGCGCCCAATACGGCCAA
hSOX10	GGCGAGGCGGACGATGACAAGTT	CCTCGATGAAGGGGCGCTTGT
hCD44	TGGCATCCCTCTTGGCCTTGG	TGAGACTTGCTGGCCTCTCCGT
hGAPDH	CAATGACCCCTTCATTGACC	GACAAGCTTCCCGTTCTCAG

Allograft experiments

FVB/N recipient mice were anesthetized using Ketamine and Xylazine. Oligodendroglioma tumor cells were dissociated with accutase and intracranially grafted into mice using a Hamilton syringe and stereotactic equipment. Injections were done at coordinates 2 mm anterior and 1.5 mm lateral of the right hemisphere relative to Bregma, at a depth of 3 mm.

Ionizing Radiation

Mice and cells were placed in a cesium-137 source (J.L. Shephard & Associates) irradiator. Mice were shielded with iron collimators to focus the beam to the brain. Mice were given cranial irradiation of single dose of 10 Gy, or 10 fractions of 2 Gy, delivered at a rate of 5 fractions per week, 1 fraction per day for 2 weeks (total 10 Gy). Cells were irradiated using a single dose of 10 Gy.

Author Manuscript Author Manuscript Author Manuscript Author Manuscript

Drug treatment

AZD1480 powder was purchased from ChemieTek (Indianapolis, IN) and resuspended before each administration in water supplemented with 0.5% hypromellose (Sigma #H3785) and 0.1%Tween-80 (Sigma #P4780). Brief sonication ensured a uniform suspension before delivery to mice. Mice were given 30 mg/kg drug treatment or vehicle by oral gavage daily for eight days.

Flow cytometry

Cells were dissociated briefly with accutase to obtain single cell suspensions. Samples were incubated for 20 min on ice with DyLight 800 viability dye (Thermo Scientific) in PBS. Cells were washed with autoMACS buffer (PBS with BSA, EDTA and azide) and then incubated for 30 min on ice in autoMACS buffer with 1:100 Brilliant Violet 421 anti-mouse CD140A (BD Biosciences) and 1:100 APC anti-mouse/human CD44 (Biolegend). Cells were washed once, fixed with BD cytofix for 30 min on ice, washed again until analysis with an LSRII flow cytometer (BD Biosciences). For intracellular p-STAT3 staining, cells were permeabilized with cold Perm Buffer III (BD Biosciences) for 30 min after fixation, and then incubated with 1:10 PE anti-pSTAT3 (pY705) for 30 min. Cells were washed with autoMACS buffer once, before flow analysis.

CyQuant proliferation assay

Five-day post-irradiated (or control) cells were plated at 3000 cells per well in 96-well polyornithine/laminin coated plates in NB media. Temozolomide (100μM) was added a day after plating, and DNA content was analyzed four days later, using the CyQuant NF proliferation assay (Life Technologies), as previously described (24). Fluorescent dye labels DNA that gives an indirect measure of the number of cells.

2D Motility

Cells were seeded on laminin-coated glass coverslips and subjected to IR. Four days following IR, the coverslips were then mounted on custom-built microscope-compatible imaging chambers and cells were imaged on a Nikon Eclipse Ti-E base microscope equipped with the Yokogawa CSU-X1 confocal scanner and Andor's iXon3 EMCCD camera. Brightfield images were captured every 15 min over 8 h. Cell migration time course images were compiled and cell speed was analyzed on a single cell basis with Image J Software (NIH) and Manual Tracking plugin (Fabrice P. Cordelières, Institut Curie, Orsay, France).

3D Neurosphere Invasion

Cells were seeded on non-adherent plates and subjected to IR. Four days following IR, tumorspheres were embedded in 3D matrigel gels (BD Biosciences) and mounted on custom-built microscope-compatible imaging chambers and imaged on a Nikon Eclipse Ti-E base microscope equipped with the Yokogawa CSU-X1 confocal scanner and Andor's iXon3 EMCCD camera. Brightfield images were captured every 30 min over 24 h. Invasion areas were identified and quantified using Image J Software (NIH).

Author Manuscript Author Manuscript Author Manuscript Author Manuscript

Cellular Rheology

Cells were sparsely seeded on laminin-coated glass coverslips and subjected to IR. Four days following IR, atomic force microscopy measurements were performed directly on single cells using an Asylum MFP 3D BIO inverted optical atomic force microscope mounted on a Nikon TE2000-U inverted fluorescent microscope (Asylum Research). Cellular rheology (Young's modulus) was determined by nano-indenting single cells with low force (below 2 nN) to ensure shallow cell indentation using calibrated Si3N4 cantilevers (60 μN/nm) modified with a 5 μm borosilicate microsphere (Novascan Tech.). The resulting force-distance curves were used to derive the elastic modulus of cells by fitting Hertz model to the curves with the Igor Pro AFM Software.

Statistical Tests

Statistical tests were performed using GraphPad Prism v6.0 software. Statistical analyses for experiments with two groups were performed using Student's t-test. Statistical analyses for experiments with more than two groups were performed using one-way ANOVA with Tukey's multiple comparisons test. Kaplan Meier survival analysis was conducted and the p value of the comparison between survival curves was determined to be significant by the log-rank (Mantel-Cox) test.

Results

OPC-derived HGG has Proneural Character

To study the effects of radiation on murine gliomas, we first compared protein and gene expression in tumors arising in two genetically engineered mouse models for glioma (22,23). We chose a mouse model (ERB/p53$^{-/-}$) predisposed to oligodendroglioma (22), the most proneural of gliomas (8), that we previously showed is derived from oligodendroglial progenitor cells (OPCs) (24). We compared the ERB/p53$^{-/-}$ tumors to those of an astrocyte-derived model for glioma driven by GFAP-HRAS^{V12D}(G-RAS) (23,25). Gliomas mutant for isocitrate dehydrogenase 1/2 (IDH1/2) do not undergo a mesenchymal transition (11), and ERB/p53$^{-/-}$ tumors are wild-type for IDH1 (data not shown). Immunofluorescent staining of ERB/p53$^{-/-}$ tumors showed high levels of SOX10 and PDGFRα proteins, known markers of OPCs and human proneural HGGs (6,26), compared to the low levels observed in the G-RAS model (Fig. 1A-B). Levels of the cell surface glycoprotein CD44, a marker of human mesenchymal HGGs (6,10), were significantly lower in ERB/p53$^{-/-}$ versus G-RAS gliomas (Fig. 1A-B). Preparation of whole brain protein lysates from tumor-bearing animals demonstrated that CD44-expressing mesenchymal (G-RAS) gliomas also showed increased abundance of phosphorylated STAT3, a known driver of PMT (16), relative to PDGFRα-expressing proneural HGGs (Fig. 1C).

RT-PCR of RNA from tumors confirmed higher expression of *Sox10* and *Pdgfra* mRNAs in proneural HGGs compared to mesenchymal tumors and normal wild-type (WT) brain (Fig. 1D). Relative mRNA expression for known markers of human mesenchymal tumors (*CD44*, Vimentin (*Vim*), and transforming growth factor β1 (*Tgfb1*), Chitinase-3-like protein 1 (*Chi3l1* – mouse homologue for the human *YKL-40* gene) and Podoplanin (*Pdpn*) (6)) were elevated in mesenchymal murine gliomas compared to both proneural tumors and WT

Author Manuscript Author Manuscript Author Manuscript Author Manuscript

mouse brain (Fig. 1D and Supplementary Fig. S1A). Our data demonstrate that OPC- and astrocyte-derived murine gliomas display proneural and mesenchymal phenotypes respectively.

In Vivo Radiation of Proneural Murine HGG Induces PMT

To study the effect of cranial radiation in mice with proneural HGGs (ERB/p53$^{-/-}$), we analyzed proneural and mesenchymal markers in tumors from symptomatic animals, seven days after a single 10 Gy dose of ionizing radiation (IR). Radiation reduced levels of proneural proteins (SOX10, PDGFRα) and increased abundance of the mesenchymal marker CD44 (Fig. 2A-B). Immunoblotting of protein lysates from tumors demonstrated reduced levels of PDGFRα following radiation (Supplementary Fig. S2A). Gene expression analysis confirmed that radiation reduced mRNA levels of proneural genes *Sox10* and *Pdgfra*, and increased expression of mesenchymal genes *CD44*, *Vim* and Fibronectin1 (*Fn1*) (Fig. 2C).

To better model the radiation regimen of patients, we also irradiated symptomatic mice with five consecutive daily doses of fractionated radiation (2 Gy) each week for two weeks. Fractionated radiation led to improvement in median survival (81.5 versus 60 days – Supplementary Fig. S2B). Similar to a single 10 Gy dose of radiation, tumors treated with fractionated radiation showed increased levels of SOX10 and PDGFRα proteins, and decreased levels of CD44 (Supplementary Fig. S2C).

Irradiation Induces a Sustained Cell-intrinsic PMT in HGG Cells

Both cell-intrinsic changes as well as extrinsic cues from the tumor microenvironment can induce a PMT in glioma (10,21). To determine whether radiation-induced PMT occurs in a cell-intrinsic manner, we isolated tumor cells from mice with proneural HGGs, and irradiated low-passage tumor cells *in vitro*. Immunoblotting and real-time PCR analyses revealed a PMT starting three days post-irradiation (Supplementary Fig. S3A-B). Based on these results, we subsequently analyzed tumor cells at five days post-irradiation. RT-PCR analysis showed significant upregulation of a panel of mesenchymal genes (*CD44*, *Tgfb1*, *Fn1*, *Chi3l1*, *Vim*, *Slug*, *Snail*, *Twist*) in irradiated murine proneural HGG cells five days following radiation (10 Gy), compared to non-irradiated controls (Fig. 3A). Consistent with observations by others (21), we demonstrated that radiation of proneural human GBM cells led to reduced expression of *SOX10* and increased expression of *CD44* mRNAs (Supplementary Fig. S3C). To confirm that a homogenous population of PDGFRα+ tumor cells shows a similar response to irradiation, we acutely sorted PDGFRα+ cells isolated from a murine proneural HGG tumor and subjected these cells to irradiation. Immunoblotting results verified that, similar to heterogeneous proneural tumor cultures, we observed increased STAT3 activation and reduced levels of PDGFRα in irradiated cells compared to non-irradiated cells (Supplementary Fig. S3D). These data demonstrate radiation induces a cell-intrinsic PMT in mouse and human proneural HGG cells and that PDGFRα+ tumor cells alone can undergo a PMT.

We next conducted a two-week time course analysis by flow cytometry, using PDGFRα and CD44 as markers of proneural and mesenchymal phenotypes, respectively. Irradiated murine HGG cells maintained a high fraction of CD44+ cells and a low fraction of PDGFRα+ cells

Author Manuscript Author Manuscript Author Manuscript Author Manuscript

two weeks post-irradiation, compared to control non-irradiated cells (Fig. 3B). Hence, the cell-intrinsic radiation-induced PMT is maintained durably over time.

Radiation-induced PMT is Associated with Therapy-Resistance

To determine whether proneural HGG cells undergoing PMT display increased invasion, we measured migration and 3D invasion of cells following radiation. Mouse and human proneural HGG cells were exposed to a single dose of radiation, and mounted onto chambers for time-lapse imaging four days following irradiation. Irradiated proneural HGG cells undergoing PMT showed higher motility than non-irradiated cells (Fig. 4A). Similarly, irradiated cells were allowed to form tumorspheres, and embedded in Matrigel four days post-irradiation to measure invasiveness. Proneural HGG tumorspheres exposed to radiation were more invasive than non-irradiated tumorspheres (Fig. 4B). Using atomic force microscopy, we found that irradiated mouse and human HGG cells displayed reduced cellular stiffness four days following radiation, compared to nonirradiated control cells (Supplementary Fig S4A).

To study temozolomide resistance following radiation, proneural murine and human HGG cells were subjected to a single dose of radiation, equal numbers of live cells were replated four days post-irradiation, incubated with temozolomide (100 μM) and proliferation was measured using a CyQuant proliferation assay. As expected, irradiated cells demonstrated reduced proliferation compared to non-irradiated control cells (Supplementary Fig. S4B). Importantly, mouse and human HGG cells post-irradiation displayed temozolomide resistance compared to non-irradiated control cells (Fig. 4C). These results suggest that resistance to temozolomide and reduced cellular stiffness in post-irradiated mesenchymal tumor cells enable survival and migration in the tumor microenvironment, promoting malignant progression and recurrence.

STAT3 as a driver of radiation-induced PMT in HGG

STAT3 is a master regulator of the glioma mesenchymal transcriptional network in human HGGs (16), and activated STAT3 drives tumorigenicity and self-renewal of GBM cancer stem cells (27,28). Primary cultures from three murine HGGs and a human proneural GBM showed increased levels of phosphorylated STAT3 (Fig. 5A) at five days following radiation. Levels of proneural proteins PDGFRα and SOX10 showed a corresponding decrease, consistent with a PMT (Fig. 5A).

We next investigated whether the activation of STAT3 was durable. Phospho-flow analysis of cells five days post-irradiation showed increased levels of phosphorylated STAT3, consistent with immunoblotting results. The increased level of phosphorylated STAT3 was lost at later time points (Supplementary Fig. S5A), suggesting that radiation induces a transient activation of STAT3 that is sufficient to trigger durable activation of downstream mesenchymal transcriptional targets.

Pharmacological Inhibition of JAK2-STAT3 Signaling Prevents PMT in HGG Cultures

The transient nature of STAT3 phosphorylation in response to radiation raises questions as to whether STAT3 is a driver of PMT in response to radiation. Janus kinase 2 (JAK2)

Author Manuscript Author Manuscript Author Manuscript Author Manuscript

phosphorylates and activates STAT3(29). The JAK2 inhibitor AZD1480 and the dual JAK1/2 inhibitor ruxolitinib (INCB018424) have been tested in clinical trials and shown to block down-stream activation of STAT3 (30-32). To assess pharmacological blockade of STAT3 phosphorylation, we first incubated murine proneural HGG cells with increasing doses of AZD1480 (0.5-2.0 μM) or ruxolitinib (0.25-2.0 μM), stimulating STAT3 signaling with 10 ng/ml oncostatin M 15 min before cell harvest (Supplementary Fig. S5B). AZD1480 and ruxolitinib significantly inhibited STAT3 phosphorylation at 1.0 μM and 0.5 μM respectively. A similar experiment conducted by incubating murine proneural HGG cells with each inhibitor for five days demonstrated a sustained inhibition of STAT3 activation for five days post-treatment (Supplementary Fig. S5C).

Treatment of cells with either JAK inhibitor, in combination with radiation, prevented PMT five days post-irradiation. Immunoblotting showed that irradiated cells treated with AZD1480 or ruxolitinib had a corresponding rescue of SOX10 protein levels (Fig. 5B and Supplementary Fig. S5D). Using the more specific JAK2 inhibitor AZD1480, we found that cells treated with AZD1480 in combination with radiation failed to increase mesenchymal gene expression compared to control irradiated cells not treated with AZD1480 (Fig. 5C). Combination treatment of AZD1480 with radiation also abrogated the invasiveness of radiated human GBM5 tumorspheres (Fig. 5D). To study the *in vivo* survival benefit of combination treatment of AZD1480 and radiation, we allografted PDGFRα+ proneural HGG cells into cohorts of FVB/N mice. Irradiated mice showed a survival benefit compared to non-irradiated mice ($p<0.001$). Further, an additional eight-day treatment regimen with AZD1480 (30 mg/kg/day) resulted in a significant extension of survival compared to irradiation alone ($p<0.01$) (Fig. 5E). These results show that pharmacological inhibition of JAK2 effectively reduces phosphorylation of STAT3, associated with blockade of radiation-induced PMT in murine proneural HGG cells.

Discussion

Despite aggressive treatment, patients with HGGs invariably relapse, and prognosis remains dismal. Recurrent tumors are often refractory to further therapy, showing both a high degree of invasiveness and a shift to a mesenchymal gene signature. Radiation remains an integral part of standard of care in HGG patients. Does radiation as a treatment contribute to recurrence and increased aggressiveness in tumors at relapse?

Using a genetically engineered model for proneural HGG, we show that radiation induces a robust and durable PMT *in vivo*. Oligodendroglioma represents the most proneural of gliomas (8), hence we chose a mouse model for oligodendroglioma for these studies. Nevertheless, to extend our findings to human proneural glioma, we show similar results in a primary culture from a human proneural glioma (GBM5 cells), also confirming results of a previous study (21).

Components of the tumor microenvironment have been suggested to promote a mesenchymal signature (6). Areas of higher necrosis are associated with more mesenchymal character (19), and microglia/macrophages have been proposed as a source of TNFα paracrine signaling to tumor cells (10). In previous studies, tumor cells isolated after

Author Manuscript Author Manuscript Author Manuscript Author Manuscript

irradiation *in vivo* showed a PMT on a transcriptional level (20), but it remains unclear if PMT induction was due to the tumor microenvironment interactions or was cell-intrinsic. While our results demonstrate that exposing isolated primary tumor cells to radiation induces a cell-intrinsic PMT, they do not exclude the possibility that tumor microenvironment components can modulate the mesenchymal phenotype.

Prior analyses of the radiation-induced PMT were limited to 6 hr for mouse HGGs *in vivo* (20) and five days for human GBM cells *in vitro* (21). We demonstrate a durable PMT at two weeks following radiation of proneural murine HGG *in vivo* and *in vitro*. Further, we demonstrated that the mesenchymal transition was associated with temozolomide resistance, increased invasiveness, and reduced cell stiffness, findings also observed in human proneural GBM5 cells. Thus, radiation treatment may drive a mesenchymal signature associated with treatment resistance and increased invasiveness at relapse.

We also identified STAT3 as a driver for radiation-induced PMT, supporting previous findings that STAT3 is a master regulator of the mesenchymal transcriptional network (16). Interestingly, phosphorylation of STAT3 occurred transiently in irradiated tumor cells that nevertheless showed sustained expression of the mesenchymal transcriptional network. Since HGG patients receive six weeks of fractionated radiation, this transient activation of STAT3 may be repeated at each cycle, conceivably expanding a population of radioresistant cells with a therapy-resistant mesenchymal phenotype. Aldehyde dehydrogenase has also been implicated in PMT in glioma cells (21), however there are currently no selective ALDH antagonists available for clinical use (33).

To assess STAT3 as a driver of radiation-induced PMT, we tested pharmacological inhibition of JAK2 to determine whether blockade of downstream STAT3 signaling could prevent radiation-induced PMT. We showed that blockade of STAT3 activation prior to, and concurrent with radiotherapy was effective in blocking the mesenchymal transition in glioma cells, and conferred survival benefit in mice with proneural HGG tumors. Therefore, our study suggests that inhibitors of JAK2 may block radiation-induced PMT in patients receiving radiation therapy for HGG.

Supplementary Material

Refer to Web version on PubMed Central for supplementary material.

Acknowledgements

We acknowledge Davide Ruggero, Lisa Coussens, and Gabriele Bergers for helpful discussions and critical review. We thank Fong Ming Koh for generously providing *Snail* and *Slug* mouse primers.

Grant Support

J.L. was supported by the National Science Scholarship by the Agency for Science, Technology and Research of Singapore and the GEMS-CTSI Graduate Student Scholar Award. S.I. was supported by the Swedish Pediatric Brain Tumor Foundation and the Swedish Childhood Cancer Foundation. Y.A.M. was supported by NSF GRFP and NIH F31CA180422. This work was supported by U54CA163155 (W.A.W., A.I.P., V.M.W.), the Samuel Waxman Cancer Research Foundation (W.A.W.), the National Brain Tumor Society 58112-01 (A.I.P.), R21NS088114 (A.I.P.), the TDC Foundation (A.I.P.), and the Guggenhime Endowment Fund (A.I.P.).

Author Manuscript Author Manuscript Author Manuscript Author Manuscript

References

1. Walker, Michael D.; Alexander, Eben, Jr; Hunt, William E.; MacCarty, Collin S.; Stephen Mahaley, M., Jr; Mealey, John, Jr, et al. Evaluation of BCNU and/or radiotherapy in the treatment of anaplastic gliomas.. Journal of Neurosurgery Publishing Group. http://dxdoiorg/103171/jns19784930333
2. Stupp R, Mason WP, van den Bent MJ, Weller M, Fisher B, Taphoorn MJB, et al. Radiotherapy plus concomitant and adjuvant temozolomide for glioblastoma. N Engl J Med. 2005; 352:987–96. [PubMed: 15758009]
3. Wen PY, Kesari S. Malignant Gliomas in Adults. N Engl J Med. 2008; 359:492–507. [PubMed: 18669428]
4. DeAngelis LM. Chemotherapy for Brain Tumors — A New Beginning. N Engl J Med. 2005; 352:1036–8. [PubMed: 15758016]
5. Phillips HS, Kharbanda S, Chen R, Forrest WF, Soriano RH, Wu TD, et al. Molecular subclasses of high-grade glioma predict prognosis, delineate a pattern of disease progression, and resemble stages in neurogenesis. Cancer Cell. 2006; 9:157–73. [PubMed: 16530701]
6. Verhaak RGW, Hoadley KA, Purdom E, Wang V, Qi Y, Wilkerson MD, et al. Integrated genomic analysis identifies clinically relevant subtypes of glioblastoma characterized by abnormalities in PDGFRA, IDH1, EGFR, and NF1. Cancer Cell. 2010; 17:98–110. [PubMed: 20129251]
7. Sturm D, Witt H, Hovestadt V, Khuong-Quang D-A, Jones DTW, Konermann C, et al. Hotspot Mutations in H3F3A and IDH1 Define Distinct Epigenetic and Biological Subgroups of Glioblastoma. Cancer Cell. 2012; 22:425–37. [PubMed: 23079654]
8. Cooper LAD, Gutman DA, Long Q, Johnson BA, Cholleti SR, Kurc T, et al. The proneural molecular signature is enriched in oligodendrogliomas and predicts improved survival among diffuse gliomas. PLoS ONE. 2010; 5:e12548. [PubMed: 20838435]
9. Guan, X.; Vengoechea, J.; Zheng, S.; Sloan, AE.; Chen, Y.; Brat, DJ., et al. PLoS ONE. Vol. 9. Public Library of Science; 2014. Molecular Subtypes of Glioblastoma Are Relevant to Lower Grade Glioma.; p. e91216
10. Bhat KPL, Balasubramaniyan V, Vaillant B, Ezhilarasan R, Hummelink K, Hollingsworth F, et al. Mesenchymal Differentiation Mediated by NF-κB Promotes Radiation Resistance in Glioblastoma. Cancer Cell. 2013
11. Lai A, Kharbanda S, Pope WB, Tran A, Solis OE, Peale F, et al. Evidence for Sequenced Molecular Evolution of IDH1 Mutant Glioblastoma From a Distinct Cell of Origin. Journal of Clinical Oncology. 2011; 29:4482–90. [PubMed: 22025148]
12. Lu KV, Chang JP, Parachoniak CA, Pandika MM, Aghi MK, Meyronet D, et al. VEGF inhibits tumor cell invasion and mesenchymal transition through a MET/VEGFR2 complex. Cancer Cell. 2012; 22:21–35. [PubMed: 22789536]
13. Carbonell WS, DeLay M, Jahangiri A, Park CC, Aghi MK. 1 Integrin Targeting Potentiates Antiangiogenic Therapy and Inhibits the Growth of Bevacizumab-Resistant Glioblastoma. Cancer Res. 2013; 73:3145–54. [PubMed: 23644530]
14. Polyak K, Weinberg RA. Transitions between epithelial and mesenchymal states: acquisition of malignant and stem cell traits. Nat Rev Cancer. 2009; 9:265–73. [PubMed: 19262571]
15. Tam, WL.; Weinberg, RA. Nat Med. Vol. 19. Nature Publishing Group; 2013. The epigenetics of epithelial-mesenchymal plasticity in cancer.; p. 1438-49.
16. Carro MS, Lim WK, Alvarez MJ, Bollo RJ, Zhao X, Snyder EY, et al. The transcriptional network for mesenchymal transformation of brain tumours. Nature. 2009; 463:318–25. [PubMed: 20032975]
17. Bhat KPL, Salazar KL, Balasubramaniyan V, Wani K, Heathcock L, Hollingsworth F, et al. The transcriptional coactivator TAZ regulates mesenchymal differentiation in malignant glioma. Genes Dev. 2011; 25:2594–609. [PubMed: 22190458]
18. Niola F, Zhao X, Singh D, Sullivan R, Castano A, Verrico A, et al. Mesenchymal high-grade glioma is maintained by the ID-RAP1 axis. J Clin Invest. 2013; 123:405–17. [PubMed: 23241957]

Author Manuscript Author Manuscript Author Manuscript Author Manuscript

19. Cooper LAD, Gutman DA, Chisolm C, Appin C, Kong J, Rong Y, et al. The tumor microenvironment strongly impacts master transcriptional regulators and gene expression class of glioblastoma. American Journal Of Pathology. 2012; 180:2108–19. [PubMed: 22440258]
20. Halliday J, Helmy K, Pattwell SS, Pitter KL, LaPlant Q, Ozawa T, et al. In vivo radiation response of proneural glioma characterized by protective p53 transcriptional program and proneural-mesenchymal shift. Proc Natl Acad Sci USA. 2014; 111:5248–53. [PubMed: 24706837]
21. Mao P, Joshi K, Li J, Kim S-H, Li P, Santana-Santos L, et al. Mesenchymal glioma stem cells are maintained by activated glycolytic metabolism involving aldehyde dehydrogenase 1A3. Proc Natl Acad Sci USA. 2013; 110:8644–9. [PubMed: 23650391]
22. Weiss WA, Burns MJ, Hackett C, Aldape K, Hill JR, Kuriyama H, et al. Genetic determinants of malignancy in a mouse model for oligodendroglioma. Cancer Res. 2003; 63:1589–95. [PubMed: 12670909]
23. Ding H, Roncari L, Shannon P, Wu X, Lau N, Karaskova J, et al. Astrocyte-specific expression of activated p21-ras results in malignant astrocytoma formation in a transgenic mouse model of human gliomas. Cancer Res. 2001; 61:3826–36. [PubMed: 11325859]
24. Persson AI, Petritsch C, Swartling FJ, Itsara M, Sim FJ, Auvergne R, et al. Non-stem cell origin for oligodendroglioma. Cancer Cell. 2010; 18:669–82. [PubMed: 21156288]
25. Shannon P, Sabha N, Lau N, Kamnasaran D, Gutmann DH, Guha A. Pathological and molecular progression of astrocytomas in a GFAP:12 VHa-Ras mouse astrocytoma model. Am J Pathol. 2005; 167:859–67. [PubMed: 16127163]
26. Hughes, EG.; Kang, SH.; Fukaya, M.; Bergles, DE. Nat Neurosci. Vol. 16. Nature Publishing Group; 2013. Oligodendrocyte progenitors balance growth with self-repulsion to achieve homeostasis in the adult brain.; p. 668-76.
27. Sherry MM, Reeves A, Wu JK, Cochran BH. STAT3 Is Required for Proliferation and Maintenance of Multipotency in Glioblastoma Stem Cells. 2009; 27:2383–92. [PubMed: 19658181]
28. Kim, E.; Kim, M.; Woo, D-H.; Shin, Y.; Shin, J.; Chang, N., et al. Cancer Cell. Vol. 23. Elsevier; 2013. Phosphorylation of EZH2 Activates STAT3 Signaling via STAT3 Methylation and Promotes Tumorigenicity of Glioblastoma Stem-like Cells.; p. 839-52.
29. Schindler C, Darnell JE. Transcriptional responses to polypeptide ligands: the JAK-STAT pathway. Annu Rev Biochem. 1995; 64:621–51. [PubMed: 7574495]
30. Verstovsek S, Kantarjian H, Mesa RA, Pardanani AD, Cortes-Franco J, Thomas DA, et al. Safety and Efficacy of INCB018424, a JAK1 and JAK2 Inhibitor, in Myelofibrosis. N Engl J Med. 2010; 363:1117–27. [PubMed: 20843246]
31. Hedvat M, Huszar D, Herrmann A, Gozgit JM, Schroeder A, Sheehy A, et al. The JAK2 Inhibitor AZD1480 Potently Blocks Stat3 Signaling and Oncogenesis in Solid Tumors. Cancer Cell. 2009; 16:487–97. [PubMed: 19962667]
32. Plimack, ER.; LoRusso, PM.; McCoon, P.; Tang, W.; Krebs, AD.; Curt, G., et al. The Oncologist. Vol. 18. AlphaMed Press; 2013. AZD1480: A Phase I Study of a Novel JAK2 Inhibitor in Solid Tumors.; p. 819-20.
33. Koppaka V, Thompson DC, Chen Y, Ellermann M, Nicolaou KC, Juvonen RO, et al. Aldehyde Dehydrogenase Inhibitors: a Comprehensive Review of the Pharmacology, Mechanism of Action, Substrate Specificity, and Clinical Application. Pharmacological Reviews. 2012; 64:520–39. [PubMed: 22544865]

Author Manuscript Author Manuscript Author Manuscript Author Manuscript

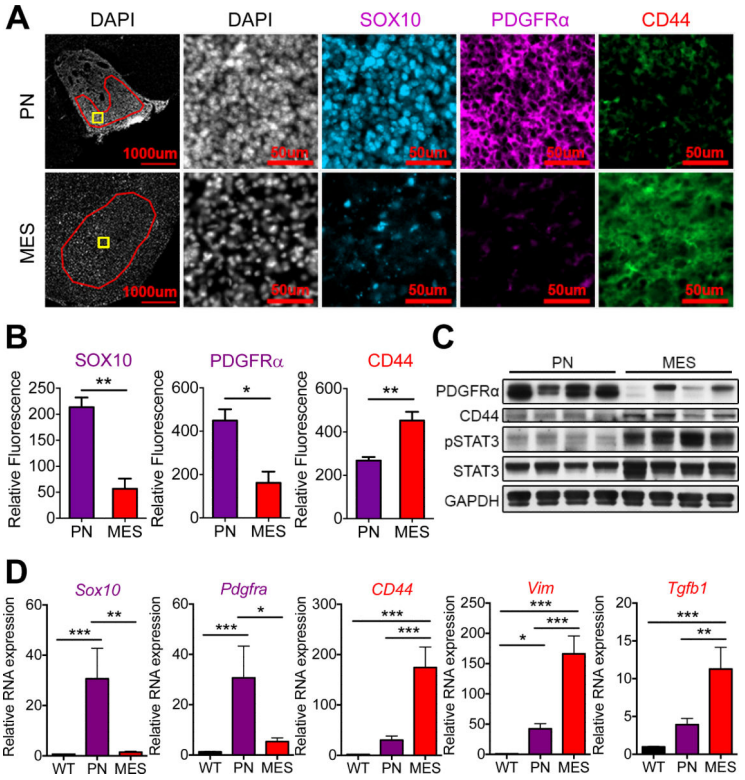

Figure 1. OPC- and astrocyte-derived transgenic murine glioma models display proneural and mesenchymal characteristics, respectively

(A) Immunofluorescence of proneural markers (SOX10, PDGFRα) and mesenchymal marker (CD44) in OPC-derived HGG model (ERB/p53$^{-/-}$; PN) and astrocyte-derived glioma model (G-RAS; MES). Red region of interest exclude necrotic regions and tumor edges for relative fluorescence quantification. Yellow boxes indicate regions shown in higher magnification images in (A). Scale bars: 1000 μm and 50 μm. (B) Fluorescent intensity quantification of SOX10, PDGFRα and CD44 in tumors (region of interest marked red in (A)) in proneural (purple) and mesenchymal (red) murine glioma models. (C) Immunoblotting for PDGFRα, CD44, and phosphorylated STAT3 of whole brain lysates from mice with proneural and mesenchymal gliomas. (D) Relative mRNA expression by RT-PCR of proneural genes *Sox10* and *Pdgfra*, and mesenchymal genes *CD44*, *Vim* and *Tgfb1* in isolated proneural (purple) and mesenchymal (red) tumors compared to normal wild-type (WT) mouse brain. * $P < 0.05$, ** $P < 0.01$, *** $P < 0.001$.

Author Manuscript Author Manuscript Author Manuscript Author Manuscript

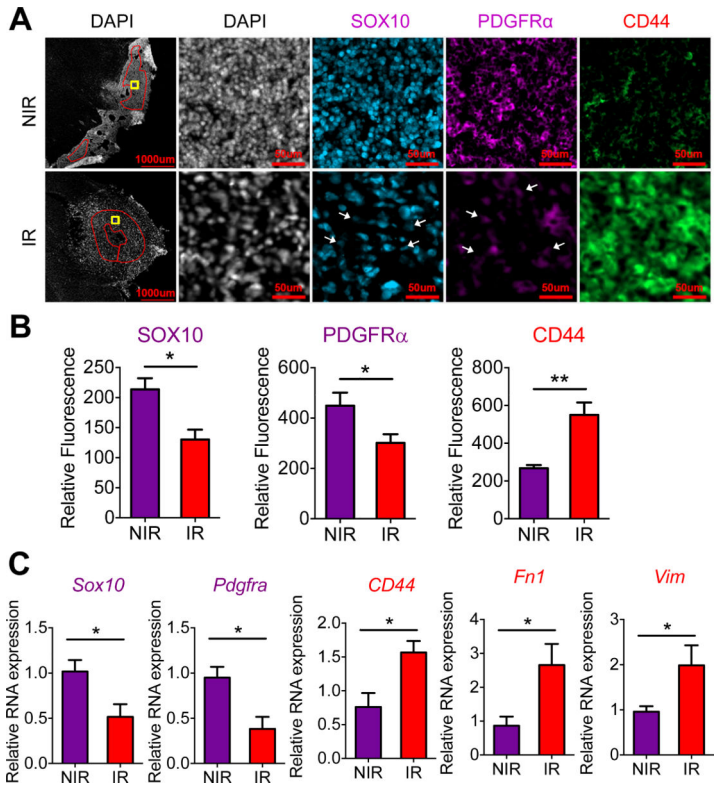

Figure 2. *In vivo* radiation induces a PMT in a proneural HGG murine model

(A) Immunofluorescence of proneural markers (SOX10, PDGFRα) and mesenchymal marker (CD44) in proneural HGG mice seven days following cranial ionizing radiation (IR; 10 Gy) versus control non-irradiated (NIR) mice. Red region of interest exclude necrotic regions and tumor edges for relative fluorescence quantification. Yellow boxes indicate regions shown in higher magnification images in (A). Scale bars: 1000 μm and 50 μm. (B) Fluorescent intensity quantification of SOX10, PDGFRα and CD44 in tumors (region of interest marked red in (A)) in murine proneural HGGs seven days following IR versus non-irradiated controls. (C) Relative mRNA expression by RT-PCR of proneural genes *Sox10* and *Pdgfra*, and mesenchymal genes *CD44*, *Vim* and *Fn1* in isolated tumors from irradiated or control allograft tumors. * $P < 0.05$, ** $P < 0.01$.

Author Manuscript Author Manuscript Author Manuscript Author Manuscript

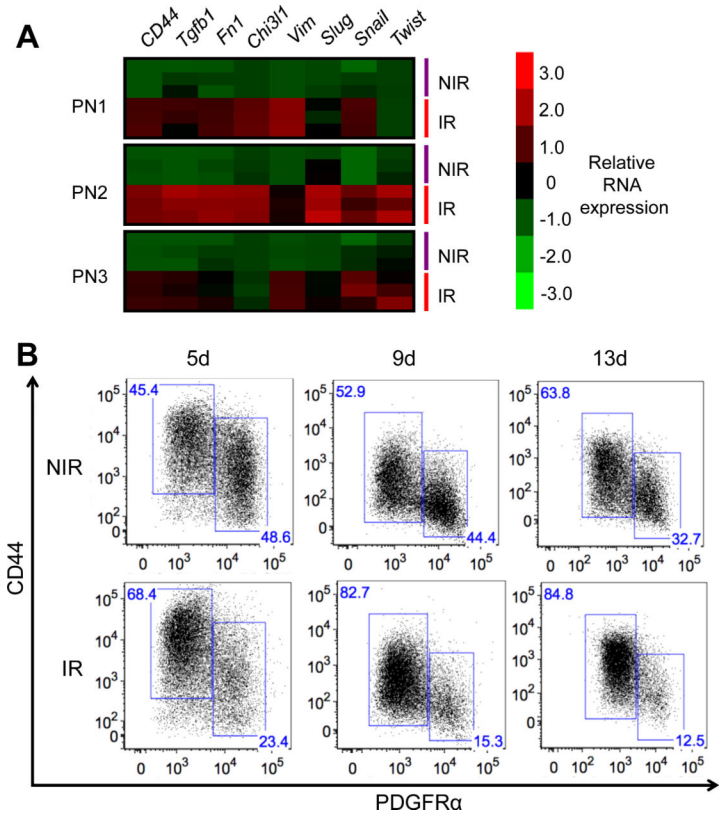

Figure 3. Radiation induces a sustained cell-intrinsic mesenchymal transition in proneural HGG cell cultures

(A) Heatmap showing relative mRNA expression of a panel of mesenchymal genes of cultured murine proneural HGG cells (PN1-PN3) five days following IR (10 Gy), compared to control non-irradiated cells. (B) Representative flow plots of PDGFRα+ and CD44+ populations at day 5, 9 and 13 following IR (10 Gy), compared to nonirradiated murine proneural HGG cells.

Author Manuscript Author Manuscript Author Manuscript Author Manuscript

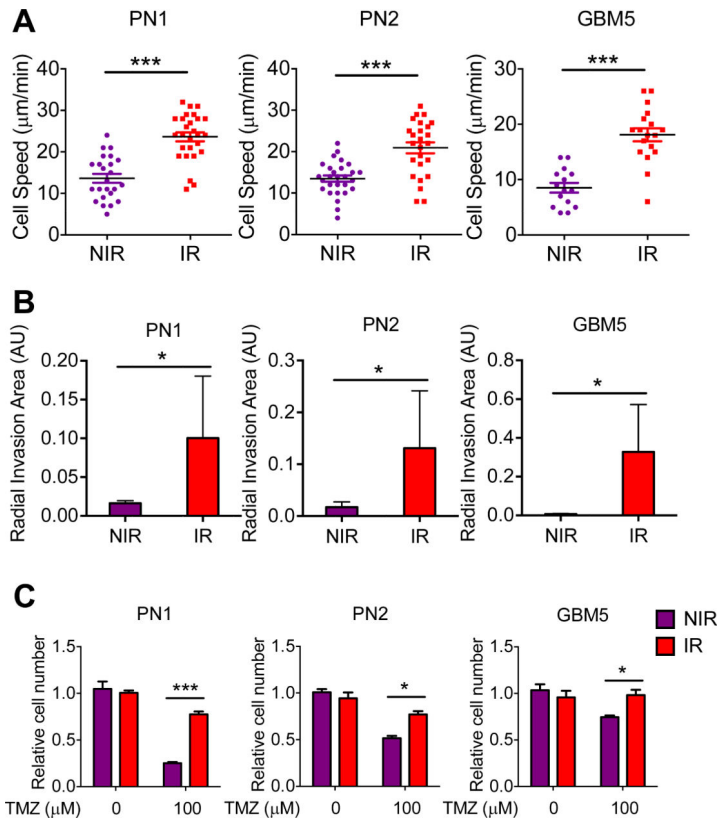

Figure 4. Radiation-induced PMT in murine and human proneural HGG cells is associated with increased motility/invasiveness and TMZ resistance

(A) Average cell speed (μm/min) by time-lapse imaging show 2D cell motility of murine (PN1-PN2) and human (GBM5) proneural HGG cultures four days following radiation, compared to non-irradiated control cultures. (B) Relative radial invasion area (arbitrary units: AU) of murine (PN1-PN2) and human (GBM5) proneural HGG tumorspheres embedded in 3D Matrigel conditions four days following radiation, compared to non-irradiated tumorspheres. (C) CyQuant DNA proliferation assay results show relative cell number in TMZ treated versus DMSO treated control murine (PN1-PN2) and human (GBM5) proneural HGG cultures, previously exposed to a single dose of IR (10 Gy). * $P < 0.05$, ** $P < 0.01$, *** $P < 0.001$.

Author Manuscript Author Manuscript Author Manuscript Author Manuscript

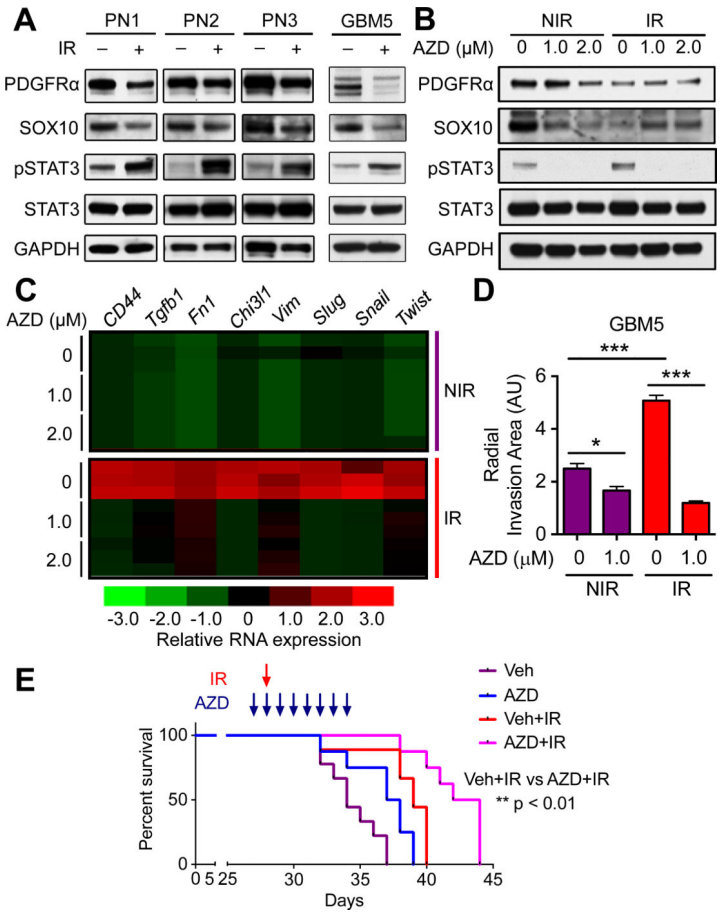

Figure 5. Pharmacological inhibition of JAK2-STAT3 signaling inhibits IR-induced PMT in proneural HGG cells and confers survival benefit *in vivo*

(A) Immunoblotting shows phosphorylated and total STAT3, and proneural markers (PDGFRα, SOX10) in cultured murine (PN1-PN3) and human (GBM5) proneural HGG cells five days following IR (10 Gy), compared to non-irradiated control cells. (B) Immunoblotting for phosphorylated and total STAT3, and proneural markers (PDGFRα, SOX10) in irradiated (10 Gy) and control cultured murine proneural HGG cells, treated in combination with JAK inhibitor AZD (1.0-2.0 μM). Inhibitor was added two hours prior to IR and cells were harvested five days following irradiation. (C) Heatmap showing relative mRNA expression of a panel of mesenchymal genes in irradiated and control murine proneural HGG cells treated in combination with JAK2 inhibitor AZD (1.0-2.0 μM) harvested at five days following irradiation. AZD was added two hours prior to IR and cells were harvested five days following IR. (D) Relative radial invasion area (arbitrary units: AU) of human (GBM5) proneural HGG tumorspheres embedded in 3D Matrigel conditions four days following combination treatment with radiation and JAK inhibition with AZD (1.0 μM), compared to non-irradiated tumorspheres. (E) Kaplan-Meier survival curves of mice injected with freshly sorted PDGFRα+ proneural HGG cells, treated with AZD1480 (30 mg/kg) or vehicle, and IR (10 Gy). * P < 0.05, ** P < 0.01, *** P < 0.001.